Pergamon

Geochimica et Cosmochimica Acta, Vol. 65, No. 23, pp. 4257–4266, 2001

0016-7037/01 $20.00 + .00

PII S0016-7037(01)00729-3

Dissolution kinetics of magnesite in acidic aqueous solution, a hydrothermal atomic force microscopy (HAFM) study: Step orientation and kink dynamics

GUNTRAM JORDAN,[1,*] STEVEN R. HIGGINS,[2] CARRICK M. EGGLESTON,[2] KEVIN G. KNAUSS,[3] and WOLFGANG W. SCHMAHL[1]

[1]Institut für Geologie, Mineralogie und Geophysik, Ruhr-Universität, 44780 Bochum, Germany
[2]Department of Geology and Geophysics, University of Wyoming, Laramie, WY 82071, USA
[3]Geoscience and Environmental Technical Division, Lawrence Livermore National Laboratories, Livermore, CA 94550, USA

(*Received January* 8, 2001; *accepted in revised form June* 8, 2001)

Abstract—The dissolution kinetics of features on the magnesite (104) surface were studied in aqueous solutions from pH 4.2 to 2 and at temperatures between 60 and 90°C by hydrothermal atomic force microscopy (HAFM). At pH = 4.2, HAFM images showed magnesite step orientations that are comparable to the step orientations on calcite. Similar to calcite (104), there is anisotropy in the step velocity, but the magnitude of the anisotropy is much greater for magnesite. Furthermore, below pH = 4.2, changes in the dominant step orientation were observed. These results are discussed in terms of a nearest neighbor kink dynamic model, and the associated kink dynamics were tested with kinetic Monte Carlo (KMC) simulations. The KMC results suggest that the kink dynamic model does not account for the experimental observations and that further details such as second-nearest neighbor interactions or surface/edge diffusion cannot be excluded from the model. The dominant step orientations at low pH also point toward mechanisms stabilizing steps along periodic bond chain directions. *Copyright © 2001 Elsevier Science Ltd*

1. INTRODUCTION

Magnesium- and calcium-bearing carbonates belong to the most important rock-forming minerals. Although calcite is one of the most common carbonates, magnesite is less abundant in nature, despite the similar solubility product of calcite and magnesite. The most common magnesium-bearing carbonate minerals are dolomite and hydrous magnesium carbonates (e.g., hydromagnesite). These observations are part of the so-called magnesite problem (Lippmann, 1973): crystallization and dissolution of magnesite appears to be strongly kinetically inhibited. This lower reactivity is thought to be a consequence of the lower water exchange rate of magnesium in contrast to calcium (Lippmann, 1973). Only a few studies have examined the heterogeneous kinetics at the magnesite–water interface (e.g., Chou et al., 1989; Pokrovsky and Schott, 1999; Pokrovsky et al., 1999). These studies were performed on mineral powders and do not provide any detailed information on the surface dissolution mechanisms. The present study was conducted to better understand the relationship between macroscopic kinetic results such as those cited above and the microscopic, site-level processes occurring at the mineral surface.

The dependence of etch pit development on carbonates on the chemical composition of the (aqueous) solution has been reported (e.g., Keith and Gilman, 1960; Thomas and Renshaw, 1965; Compton et al., 1989). More recently, atomic force microscopy (AFM) studies have given insight into the calcite etch pit morphology with monolayer resolution (e.g., Hillner et al., 1992; Stipp et al., 1994; Liang et al., 1996a,b; Park et al., 1996; Britt and Hlady, 1997; Teng and Dove, 1997; Jordan and Rammensee, 1998; Shiraki et al., 2000). For calcite (104), these studies showed three general results: (1) Far from equilibrium, at neutral to slightly acidic pH, pits show rhombohedral symmetry (i.e., pit walls are parallel to $[48\bar{1}]$ and $[\bar{4}41]$; (2) Close to equilibrium, at neutral to slightly basic pH, pits appear partially rounded. (3) Adding amino acids changes the geometrical shape of pits. There are various interpretations for the different step patterns. According to the periodic bond chain (PBC) theory (Hartman and Perdok, 1955), steps on calcite (104) following rhombohedral symmetry have been described as following directions with strong bonds (Heijnen, 1985; Paquette and Reeder, 1995). Step orientations observed after addition of amino acids were reportedly caused by adsorption of carboxylate and/or amino functional groups to specific surface sites (Teng and Dove, 1997). The aim of this study is to examine the magnesite–water interface at high spatial resolution to understand the specific behavior of monolayer steps during dissolution in acidic solutions. We will focus on the changes of step orientation on magnesite (104) as a function of pH, and we will evaluate the application of a kink dynamic model for this behavior. We focus on step kinetics and dissolution flux of magnesite in a forthcoming article.

2. EXPERIMENTAL

For the in situ experiments presented, we used a novel hydrothermal atomic force microscope (HAFM; Higgins et al., 1998). The HAFM enables investigation of the solid–liquid interface at temperatures well above the ambient boiling point of water by applying pressure to the fluid. The magnesite crystals used originated in Brumado, Brasilia. The crystals were cleaved immediately before the experiments with a blade. The crystals were affixed mechanically in the fluid cell. The fluid cell was then filled with fluid, sealed, pressurized, and heated. By use of a mass flow controller downstream of the fluid cell, flow rates of 10 to 80 g/h were established in the fluid cell. The microscope was operated in contact mode using uncoated silicon cantilevers (Nanosensors) operating in constant force mode at the lowest possible loading forces. The images obtained are presented either in height mode (i.e., darker gray scales represent lower areas) or in deflection mode (i.e., different gray scales represent differently inclined areas; in other words, the surface appears to be illuminated from the left). During experiments, the surface was searched for scan-related alterations by scan variation

* Author to whom correspondence should be addressed (guntram.jordan@ruhr-uni-bochum.de).

methods such as disengaging, variation of scan size, and scan angle. Possible scan-related surface alterations could not be found.

The solutions were prepared by adding reagent-grade HCl to 0.1 mol/L KCl in deionized water (resistivity: 18 MΩ cm), which was equilibrated with ambient CO_2. Chemical composition of the magnesite as analyzed by electron microprobe is, on average as follows: O = 60.04%, C = 20.07%, Mg = 19.75%, Ca = 0.08%, Fe 0.03%, and less Mn, Cu, and Zn. For magnesite lattice parameters, we used a = 0.46332 nm and c = 1.5015 nm (Joint Committee for Powder Diffraction Standards), ignoring any possible surface relaxation and reconstruction. However, for calcite (104), there is some evidence that the atomic surface structure could be slightly distorted (Stipp et al., 1994; Liang et al., 1996a; Fenter et al., 2000).

By experimentally determining the step velocity for highly vicinal steps and close-packed rhombohedral steps, and by employing some assumptions about site–site interactions (see below), we used a simple step model (e.g., Lauritzen, 1973; Frank, 1974; Liang et al., 1996b) to provide parameters relevant to the kink dynamics. Kinetic Monte Carlo (KMC) simulations were performed to test the applicability of the assumptions implicit to the step model of Lauritzen and Frank. The model assumes, for example, that only the nearest neighbor interactions are significant. In this one-dimensional treatment of step motion, it is also assumed that step overhangs are negligible (e.g., fig. 12 of Burton et al., 1951) and that there is no transport impedance. Therefore, a simple close-packed step edge on a (001) surface of a simple cubic crystal is made up of only three different sites: (1) sites with only one in-plane nearest neighbor, or adatom; (2) sites with two in-plane nearest neighbors, or kink sites; and (3) sites with three in-plane nearest neighbors, or step sites. Along a more complicated step edge, such as the rhombohedral steps on magnesite, there are two opposing and inequivalent kink sites. Therefore, the number of different step sites n used in the model here is 4. Each of these sites is assigned an event frequency, or rate, which represents the rate of detachment from each kind of site. For each step in the KMC simulation, the total frequency of events (ν_{tot}) was determined by the sum over n, the number of different sites, of the products of the specific site frequencies (ν_i) and the site population (N_i)

$$\nu_{tot} = \sum_{i=1}^{n} \nu_i N_i, \tag{1}$$

with n = 4. With each random number generated, an event (P_i) was chosen from the probability distribution

$$P_i = \frac{\nu_i N_i}{\nu_{tot}}. \tag{2}$$

Once the event was determined, a second random number was generated and used to select one of the N_i sites at random corresponding to that event. After the removal of the site, the site population distribution was recalculated and the random event/site selection process was repeated. In this approach, the time elapsed between events varies according to the instantaneous value of ν_{tot}. By stipulating the ν_i values and by performing the simulation over 10^5 or more time steps, phenomenological observables such as step velocity and step slope were calculated.

3. RESULTS AND DISCUSSION

3.1. Dissolution at pH = 4.2

Magnesite dissolves on (104) surfaces in water at pH = 4.2 by retreat of elementary steps, similar to the manner by which calcite dissolves in neutral to slightly acidic conditions at room temperature (Jordan and Rammensee, 1998; Shiraki et al., 2000). On the surface, two general kinds of steps occur: straight steps parallel to $[48\bar{1}]$ and $[\bar{4}41]$ at rhombohedral etch pits (Figs. 1a–c) and rough steps that are vicinal to $[48\bar{1}]$ and $[\bar{4}41]$ (Figs. 1d–f).

3.1.1. Straight Steps

The two opposing straight steps parallel to $[48\bar{1}]$ or $[\bar{4}41]$ are structurally inequivalent. The reason for the structural inequivalence is that as a result of the c-glide plane, successive (104) layers are shifted along $[42\bar{1}]$, so that the direction along succeeding molecular rows deviates by ~22° from the surface normal (Fig. 2a). On calcite, the angle is ~19°. This horizontal shift causes two adjacent steps ($[48\bar{1}]_a$ and $[\bar{4}41]_a$; see Fig. 2a) to overhang the underlying layer, and therefore, the steps are termed "acute." The other two adjacent steps ($[48\bar{1}]_o$ and $[\bar{4}41]_o$) retreat from the according position in the underlying layer by this horizontal shift and thus are termed "obtuse." This structural inequivalence of steps is depicted by the subscripts a and o. Thus, the notation for steps is G_a and G_o and, as simplification, we also use the same notation for the retreat velocities of these steps (the complete notation is shown in Fig. 2). The retreat velocity of steps reflects the structurally inequivalence. In Figures 1a–c, it can be seen that G_o steps retreat much faster than G_a steps (at the conditions applied, $G_o/G_a \geq 50$).

3.1.2. Rough Steps

In contrast to straight steps (G_o, G_a), we indicate rough steps by double subscript indices (e.g., G_{oo}, G_{aa}). These indices designate the two merging straight steps that form the rough step. Figures 1d–f shows the motion of rough steps at two intersecting pits. In Figure 1d, two pits intersect to form two new rough steps resulting from the merging of acute steps (lower left of the two pits) and obtuse steps (upper right). Five minutes later (Fig. 1e), the rough obtuse–obtuse step (G_{oo}) to the upper right already dissolved to form straight $[48\bar{1}]_o$ and $[\bar{4}41]_o$ steps again. After 11 min (Fig. 1f), the rough acute–acute step (G_{aa}) to the lower left had still not fully dissolved, in contrast to its obtuse–obtuse counterpart. In addition to G_{oo} and G_{aa} steps, a third rough step, occurring at the intersection of obtuse steps with acute steps G_{oa}, can be observed (Fig. 3). The velocity of this G_{oa} step is intermediate to acute–acute and obtuse–obtuse rough steps. Rough steps usually were observed to be rounded, although jagged steps also could be found (e.g., by becoming pinned temporarily; Jordan and Rammensee, 1998). However, G_{oo} and G_{aa} steps are generally oriented along [010], whereas G_{oa} steps follow $[42\bar{1}]$.

3.1.3. Kink Dynamics

Several authors have used a kink dynamic model to describe the motion of steps on calcite during growth and dissolution (e.g., Gratz et al., 1993; Paquette and Reeder, 1995; Liang et al., 1996b; Liang and Baer, 1997; Jordan and Rammensee, 1998; de Leeuw et al., 1999). Following these authors and the work of Lauritzen (1973) and Frank (1974), step motion is caused by double kink formation (i) and detachment at single kink sites (g). In contrast to the use of capital letters for steps and step velocities, lowercase letters are used to refer to kink-related processes. For the different kink sites g, the first subscript index defines the step, and the second, the direction of kink propagation along the step (all denotations are compiled in Fig. 2; note that at rough steps, both steps and kinks have the same subscripts).

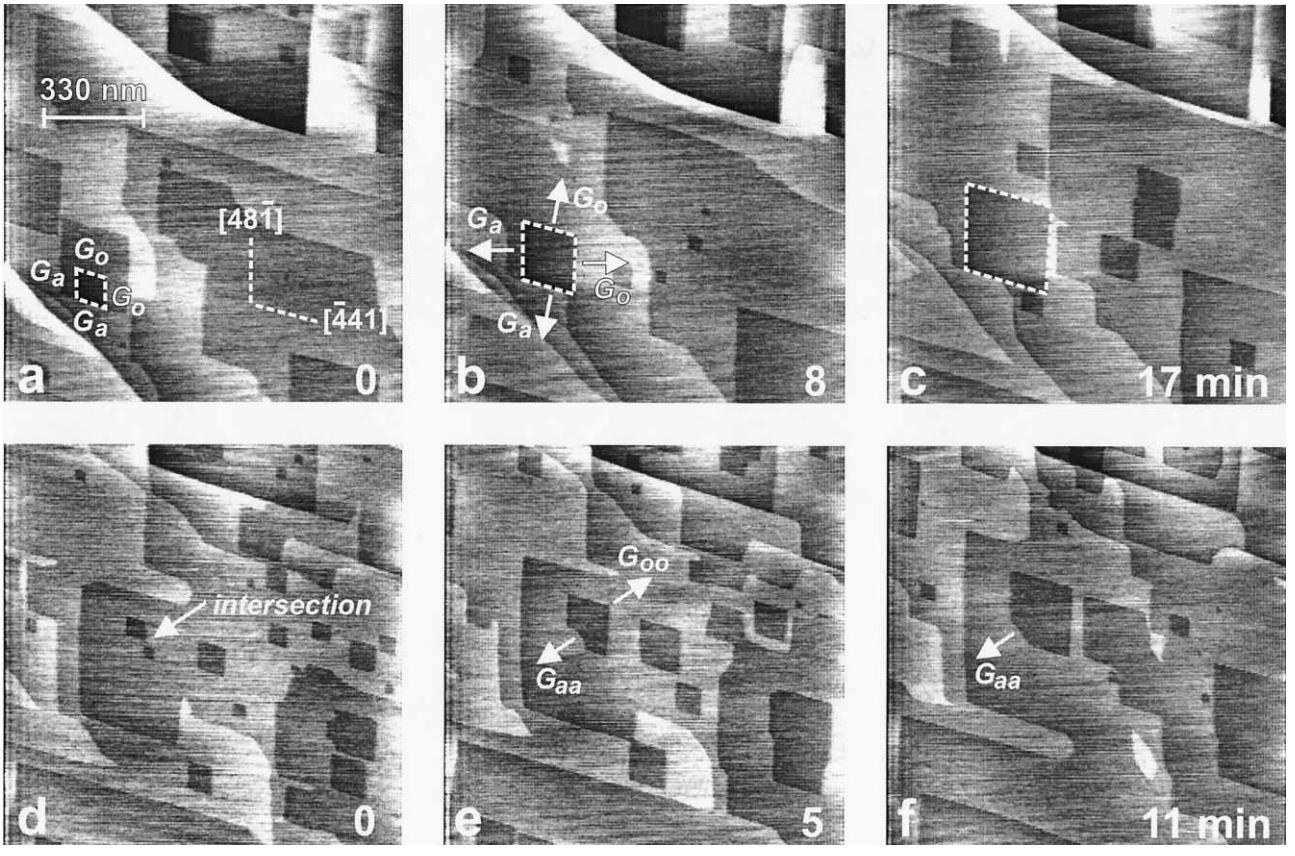

Fig. 1. Magnesite (104) surface dissolving in water (pH = 4.2 HCl ± 0.1 mol/L KCl) at 60°C. (a–c) Steps at pits (straight steps) are oriented parallel to the rhombohedral directions [48$\bar{1}$] and [$\bar{4}$41]. G_o steps retreat much faster than G_a steps. (d–f) Intersecting pits create rough steps. The retreat velocity of rough steps is inequivalent. G_{oo} steps are much faster than G_{aa} steps. The surface is shown in height mode—that is, brighter and darker gray scales represent higher and lower surface areas, respectively. Most steps shown are monolayer steps (~0.3 nm in height); however, in a few spots, as can be seen in the images, steps are merging to form double- and triple-layer steps.

According to the model of Lauritzen (1973) and Frank (1974), net detachment rates g at the two different kink sites along a step (Fig. 2a) have to be faster than the net rate of double kink formation i for the formation of straight steps. Thus, at obtuse steps, the conditions $g_{oo} \gg i_o$ and $g_{oa} \gg i_o$ must hold. In addition, as discussed below, the two net kink detachment rates at a straight step must be similar to avoid a vicinal step orientation. The relation between kink detachment rates g and double kink formation i at straight obtuse and acute steps, therefore, is $g_{oo} \approx g_{oa} \gg i_o$ and $g_{ao} \approx g_{aa} \gg i_a$, respectively. If we make the assumption that rough steps consist entirely of kink sites (see Fig. 2), these relationships provide a qualitative explanation for the observation that $G_{rough} > G_{straight}$. In other words, the rough steps may be considered to have a maximum density of kinks and therefore must retreat at a velocity proportional to the net rate of kink detachment. The straight steps, where kink populations are limited by initiation (i) and kink–kink annihilation, retreat at a somewhat lower velocity.

The kinks on a rough step are identical to kinks on a straight step as long as only nearest neighbor interactions are considered (see, e.g., g_{oa} in Fig. 2c). Considering second-nearest neighbor positions, straight-step kinks have fewer second-nearest neighbors than kinks on a rough step. Because of possibly stabilizing interactions, as discussed in 3.2.3., the net detachment rate of kinks at straight steps may be expected to be higher than that of rough steps. Paquette and Reeder (1995) further pointed out that there are differences in second-nearest neighbor coordination of g_{oa} and g_{ao} kinks. However, to enhance clarity in the following considerations, we will neglect any possible differences between g_{oa} and g_{ao} kinks.

On the basis of experimental data on calcite at pH = 9 at room temperature and KMC simulations, Liang et al. (1996c) determined net detachment rates at kink sites $g_{oo} = 330.6\ s^{-1}$, $g_{oa} = 141.2\ s^{-1}$, $g_{aa} = 60.3\ s^{-1}$, and double-kink nucleation rates $i_o = 0.301\ s^{-1}$ and $i_a = 0.129\ s^{-1}$. On magnesite, we calculated g_{oo} and g_{oa} by the retreat velocity of the rough G_{oo} and G_{oa} steps. As depicted in Figure 2b,

$$g_{oo} = G_{oo}/b \cos(103°/2) \quad (3)$$

and

$$g_{oa} = G_{oa}/b \cos(77°/2), \quad (4)$$

where b (=0.59 nm) is a lattice parameter assuming combined anion and cation detachment. Inherent in this calculation are the following assumptions: (1) rough steps are saturated in kink sites; (2) rough step kinks have net detachment rates similar to

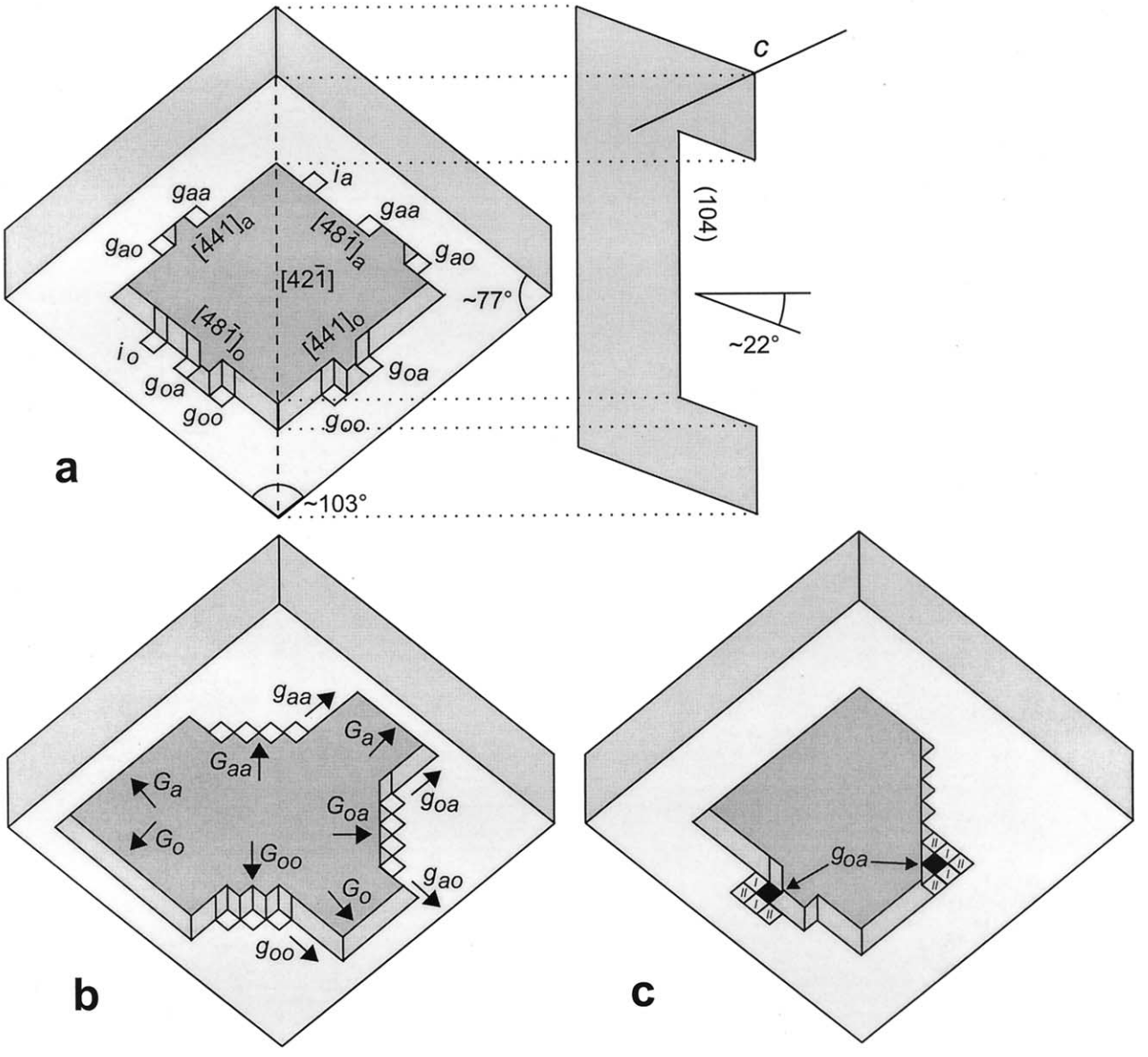

Fig. 2. Sketch showing the orientation and notation of steps and kinks on the (10$\bar{4}$) surface. In (a, left), (b), and (c), the (104) surface lies parallel to the paper plane. A section oriented along [42$\bar{1}$] (=[2$\bar{2}$1]), as depicted by the dashed line, is shown in the right part of (a). As a result of the crystal symmetry, layers parallel to (104) are shifted along [421]. Intersecting pits create rough steps (b, G_{oo}, G_{oa}, and G_{aa}). (c) Nearest neighbors (*I*) and second-nearest neighbors (*II*) of g_{oa} kinks (black) at straight steps (left side) and rough steps (right side).

the rates of the respective straight step kinks; and (3) the difference between g_{oa} and g_{ao} is negligible. Because we cannot rule out possible influences of coordination chemistry and impurities (e.g., at the jagged rough steps), the model should be regarded as a first approximation. Table 1 shows the detachment rates of g_{oo} and g_{oa} kinks and the ratio g_{oo}/g_{oa}. By measuring the velocity of straight steps G_o and applying the equation

$$G_o = b\,[i_o\,(g_{oo} + g_{oa})]^{1/2} \tag{5}$$

from Liang et al. (1996b), the double-kink nucleation rate i_o, and therefore the entire kink dynamic data set of G_o steps, becomes available (Table 1; the uncertainty of data mainly rises from uncertainties in determining G_{oo} and G_{oa}; data for acute steps can be determined analogously). However, the data of Table 1 can be tested. The kink detachment rates g_{oo} and g_{oa} and the step velocity G_o obtained by HAFM and used as input to Eqn. 5 may also be used as input parameters to a KMC model that utilizes the same assumptions that we employed in arriving at Eqns. 3 and 4. The KMC simulations therefore will provide a test of the validity of Eqn. 5 and a test of the explicit assumptions leading to Eqn. 3 and 4.

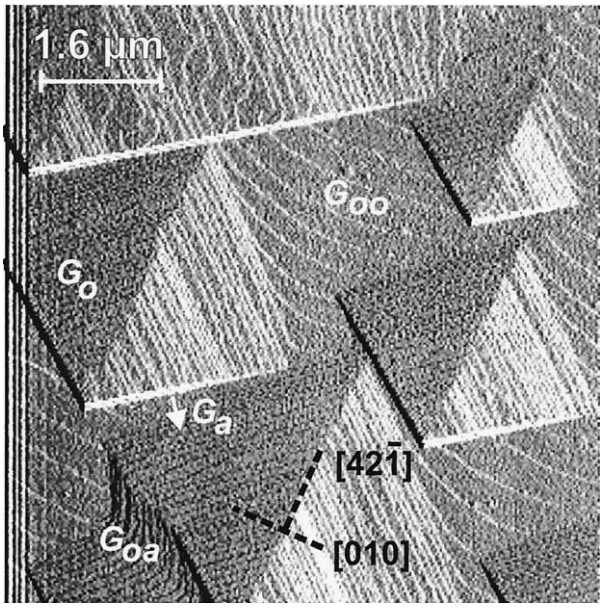

Fig. 3. Magnesite (104) surface dissolving in water (60°C, pH = 4.2 HCl, 0.1 mol/L KCl) showing a morphology dominated by step formation within the cores of etch pits. The vast anisotropy of step retreat at straight steps (G_o vs. G_a) causes steep etch pit slopes at $[481]_a$ and $[441]_a$ steps and shallow slopes at $[481]_o$ and $[441]_o$ steps. Rough steps can be seen (labeled G_{oo} and G_{oa}) between the pits. The rough steps are slightly curved but follow roughly [42$\bar{1}$] and [010]. The surface is shown in deflection mode—that is, bright and dark gray scales represent steps dropping to the left and to the right, respectively. Vertical stripes at the left margin are artificially caused by the fast scanning tip.

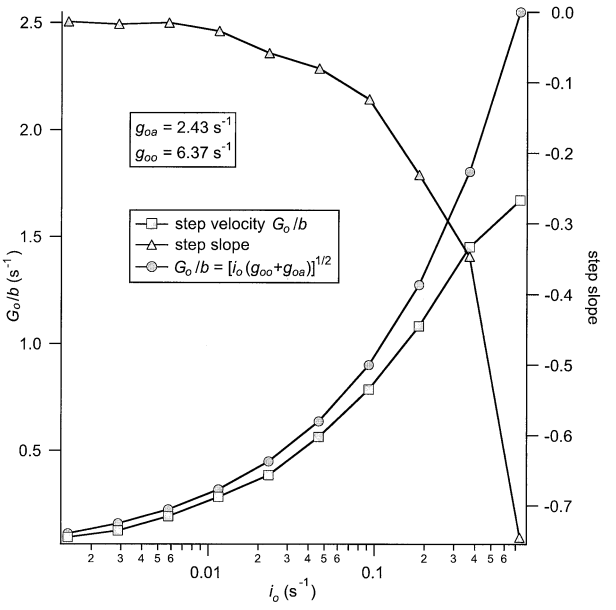

Fig. 4. Step velocity and step slope derived by one-dimensional KMC simulation by means of kink detachment rates g_{oo} and g_{oa} obtained by step velocities of rough steps (G_{oo}, G_{oa}) as input parameters. For comparison, the step velocities calculated on the basis of $G_o = b\,[i_o\,(g_{oo} + g_{oa})]^{1/2}$ (Liang et al., 1996b) are inserted.

3.1.4. Monte Carlo Simulations

In the KMC simulation, we used the following input parameters:

$$\sum_{i=1}^{n} N_i = 400;\ \nu_1 = g_{oo} = 6.37\ \text{s}^{-1};\ \nu_2 = g_{oa} = 2.43\ \text{s}^{-1};\ \nu_3 = g_{oo} + g_{oa};\ \nu_4 = i_o,$$

where ν_3 corresponds to the detachment rate of a dimer attached to a straight-step segment. Thus, by KMC simulation, step velocity G_o (perpendicular to the close-packed step orientation) and the step slope (tangent of angle between the orientation of the vicinal step and the close-packed step orientation) can be derived. The results are plotted for variable values of (i_o) in Figure 4 and compared with the step velocity G_o calculated on the basis of Eqn. 5 by means of the experimental values for g_{oo} and g_{oa} and variable values for (i_o). As shown in Table 1, from the experimental values G_o, g_{oo}, g_{oa}, and Eqn. 5, we obtain $i_o = 0.74\ \text{s}^{-1}$. From this value for i_o, the KMC simulation yields a step slope of ~0.7, which is clearly very different from the observation (Figs. 1 and 3) that these steps stay close to a slope of zero, and which therefore shows that the kink formation rate i_o derived by Eqn. 5 is too high and g_{oo} and g_{oa} are too low. As a result, the condition $g_{oo} \approx g_{oa} \gg i_o$ does not hold, which is necessary to keep steps straight and oriented along the close-packed direction. Because lower values of i_o cause not only a decrease in step vicinality but also lower velocities, any lower i_o requires larger g_{oo} and g_{oa} than derived by Eqns. 3 and 4 from G_{oo} and G_{oa}. In general, it is possible to increase g_{oo} and g_{oa} while decreasing i_o until the KMC and experimental step slopes are in agreement; however, the lack of experimental constraint on g_{oo} and g_{oa} would ensure a nonunique result. For example, we cannot easily test the validity of new values of g and i because, as shown in Figure 4, a range of different g/i ratios, all under the condition $g \gg i$, have nearly the same step slopes. These slopes are too small (~1°) to measure reliably with AFM given scanning uncertainties.

Table 1. Detachment rates g at kink sites and double kink formation rates i.[a]

	pH 4.2			pH 2
Rate	60°C	75°C	90°C	60°C
g_{oo}	1.7 ± 1.0	6.4 ± 2.8	28 ± 11	32 ± 15
g_{oa}	0.7 ± 0.4	2.4 ± 1.2	6.5 ± 2.7	1.1 ± 0.2
g_{oo}/g_{oa}	2.4 ± 1.9	2.6 ± 1.7	4.3 ± 2.4	29 ± 14
i_o	0.2 ± 0.1	0.7 ± 0.3	1.2 ± 0.4	

[a] Values are given per second, and the standard deviation is provided. Data are based on combined anion and cation detachment.

The KMC simulation is not only a test for the applicability of Eqn. 5 but also for the assumptions leading to Eqns. 3 and 4. The step slope discrepancy therefore can be regarded as an indication that the net rate of kink detachment has a definite dependence on the kink density. This may be a result of edge or surface diffusion limiting the dissolution flux, from the rough steps in particular, or of a significant interaction between second-nearest neighbors (neglecting potential violations of assumption 1 that may affect the jagged rough steps to a certain extent).

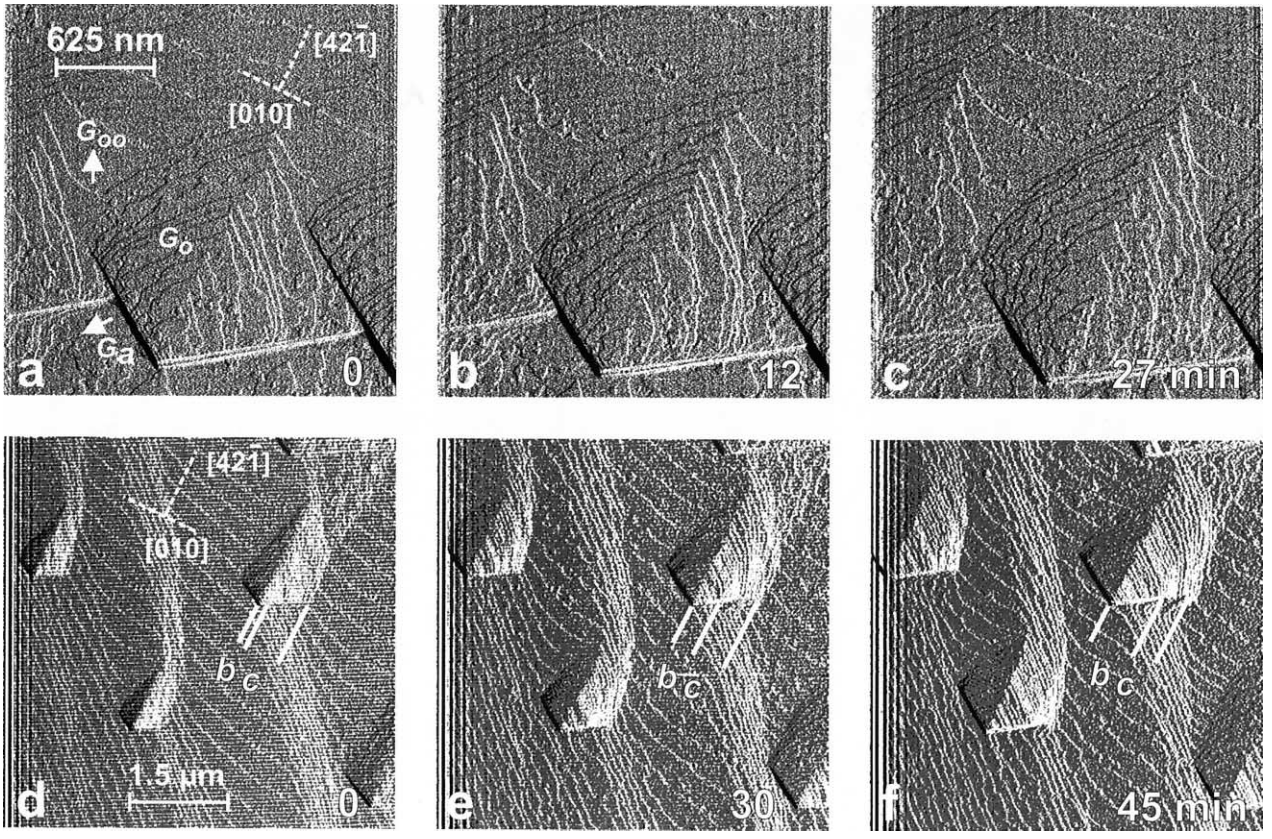

Fig. 5. Magnesite (104) surface during in situ exchange of the pH of solution at 60°C (deflection mode images, appearing as illuminated from the left side; vertical stripes at the left margin of the images are artificially caused by the fast scanning tip). (a–c) Decreasing pH from 4.2 to 3.1. In (a), solution at low pH has already entered the fluid cell indicated by an increased rate of monolayer pit formation on the terraces and by a slightly decreased angle between obtuse steps (G_o); (b) and (c) show that an altered step orientation is established. (d–f) Increasing pH from 3.1 to 4.2. In (d), the surface morphology still is almost entirely dominated by the lower pH. The orientation of obtuse steps differs clearly from the orientation of acute steps. At the center line of the pits, the new step direction (pH 4.2) has already started to establish itself (*b*). (e, f) Parts of steps at pits related to the pH = 3.1 morphology (*c*) shrink and the parts related to the new pH 4.2 solution (*b*) spread continuously.

3.2. pH Dependence

3.2.1. Step Orientation as a Function of pH

Figures 5a–c shows the magnesite (104) surface while the pH of the solution decreases from pH = 4.2 to 3.1. As the pH is lowered, the obtuse steps (G_o) roughens. The roughening of steps is primarily caused by monolayer pit nucleation on the existing terraces. The monolayer pits intersect with the retreating $[48\bar{1}]_o$ and $[\bar{4}41]_o$ steps and induce an overall increase in the kink density. This increased kink density eventually manifests itself as an increase in step vicinality. The characteristic step alignment at pH = 3.1 is reflected in a decreased angle between the two obtuse steps relative to the angle at pH = 4.2 (Fig. 5d). A return to pH = 4.2 causes the steps to reorient to the original orientation. The $[48\bar{1}]_o$ and $[\bar{4}41]_o$ step directions redevelop initially at the center line of the etch pits (i.e., where the c-glide plane intersects the surface parallel to $[42\bar{1}]$) and then spread along the obtuse steps.

The change in direction of the slow steps ($[48\bar{1}]_a$ and $[\bar{4}41]_a$ steps) is much less conspicuous (Fig. 5). However, with a decrease in the solution pH, the acute steps change direction in a manner similar to the corresponding obtuse steps with an increase in solution pH: the new step direction starts to develop at the centerline of the pit. Thus, with a decrease in pH, the newly oriented step segment starts to form at the particular end of the step to which the kinks with slower detachment rates are propagating. The new segment spreads along the step. The growing low-pH segment can be considered as an accumulation of kinks with lower detachment rates. In contrast to the observations for decreasing pH, with an increase in pH, the newly oriented acute segment starts to form at the opposite end of the step.

Decreasing the pH to below 3.1 causes the step angles to undergo additional change. Whereas at pH = 3.1 (60°C) we obtained on magnesite (104) an angle of 123 ± 3° between acute steps and 65 ± 12° between obtuse steps (Fig. 6), at pH 2 (60 °C) the angles increased/decreased to 146 ± 3°/49 ± 5°, respectively. Figure 7 shows etch pits formed by straight steps and intersectional regions formed by rough steps on magnesite at pH = 2. As at pH = 4.2, three kinds of rough steps occur: obtuse–obtuse (G_{oo}), obtuse–acute ($G_{oa} = G_{ao}$) and acute–acute (G_{aa}). Assuming an approximately constant rate of step

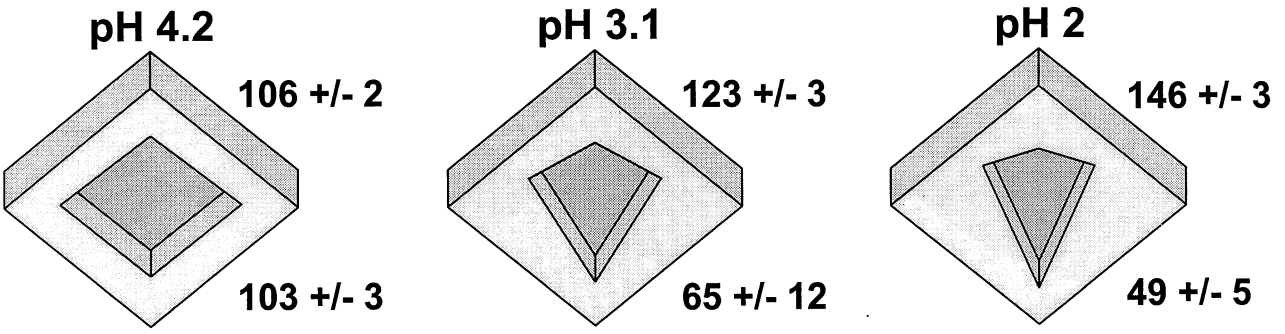

Fig. 6. Compilation of etch pit shapes (steps orientations) on the magnesite (104) surface at various pH values and 60°C. The numbers give the angles and their standard deviation between obtuse steps and acute steps.

formation I in all etch pits, the slope of the surface (i.e., the step density) is inversely proportional to the step velocity G. Because of these different velocities, surface areas with obtuse–obtuse steps (G_{oo}) and obtuse–acute steps (G_{oa}) can be observed easily. Because the orientation of rough steps remains largely unaffected by solution pH, we will treat the rough steps by the same kink dynamic model as applied at pH = 4.2.

3.2.2. Kink Dynamics

As shown by AFM images, a decrease in pH causes an increase in straight step vicinality. This increased vicinality of straight steps can be explained by an increased population of one type of kink in comparison to the population of the other. By decreasing pH, the increased population of kinks is of the slow type. A similar observation was made in a two-dimensional KMC simulation for calcite by McCoy and LaFemina (1997). Above, it was demonstrated from KMC simulation that an anisotropy in detachment rates of kink types (i.e., $g_{oo} \neq g_{oa}$) can cause a step vicinality by an accumulation of the slower of the detaching kinks. Thus, it is possible that there is a significant pH dependence of g_{oo}, as indicated by the strong pH dependence of G_{oo}, and a relatively weak pH dependence of g_{oa}. At pH = 2 and 60°C, from measuring the retreat velocities of the rough steps G_{oo} and G_{oa}, we found $g_{oa} = 0.7 \pm 0.1$ nm/s and $g_{oo} = 18.7 \pm 8.8$ nm/s (see Fig. 8). Assuming detachment in anion–cation pairs, the net detachment rates are around 1 s^{-1} and 30 s^{-1} for the g_{oa} and g_{oo} kinks, respectively. This clearly demonstrates the anisotropy of detachment rates (Table 1). In this way, the step vicinality increases with decreasing pH because of the increased anisotropy in kink detachment rates. The degree of step vicinality also depends on the rate of double kink nucleation (i_o). As shown above in the KMC simulation,

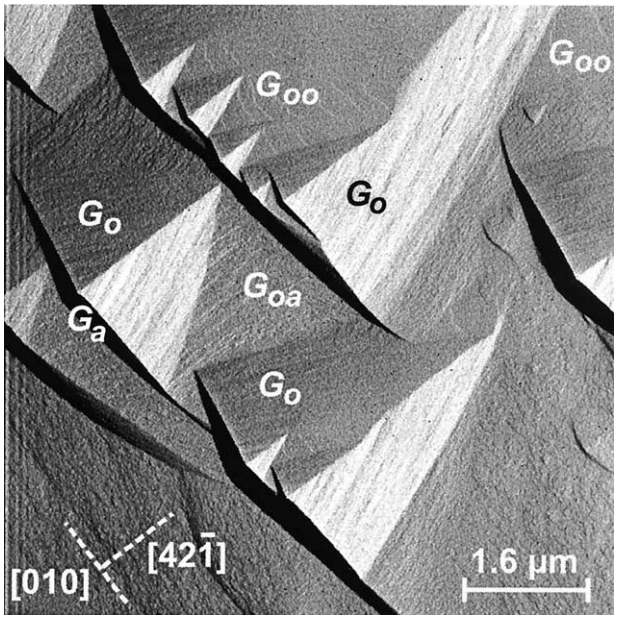

Fig. 7. Magnesite (104) surface during dissolution in pH = 2 (HCl + 0.1 mol/L KCl) at 60°C (deflection mode image appearing as illuminated from the left side; vertical stripes at the left margin are artificially caused by the fast scanning tip). The surface is composed of pits and intersectional regions; therefore, the surface morphology is dominated by terraces and by straight and rough steps. Whereas G_o and G_a steps have changed direction considerably in comparison to pH = 4.2, rough steps (G_{oo}, G_{oa}) still are oriented approximately along [42$\bar{1}$] and [010].

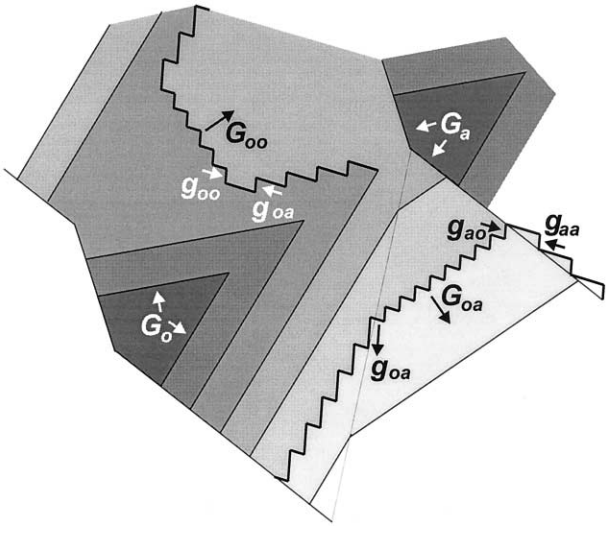

Fig. 8. Sketch showing the relation between etch pits, straight steps, rough steps, and kink detachment rates at acidic pH according to the applied kink dynamic model. The orientation of the sketch corresponds to the surface orientation in Figure 7. By measuring G_{oo} and G_{oa}, g_{oo} and g_{oa} can be estimated.

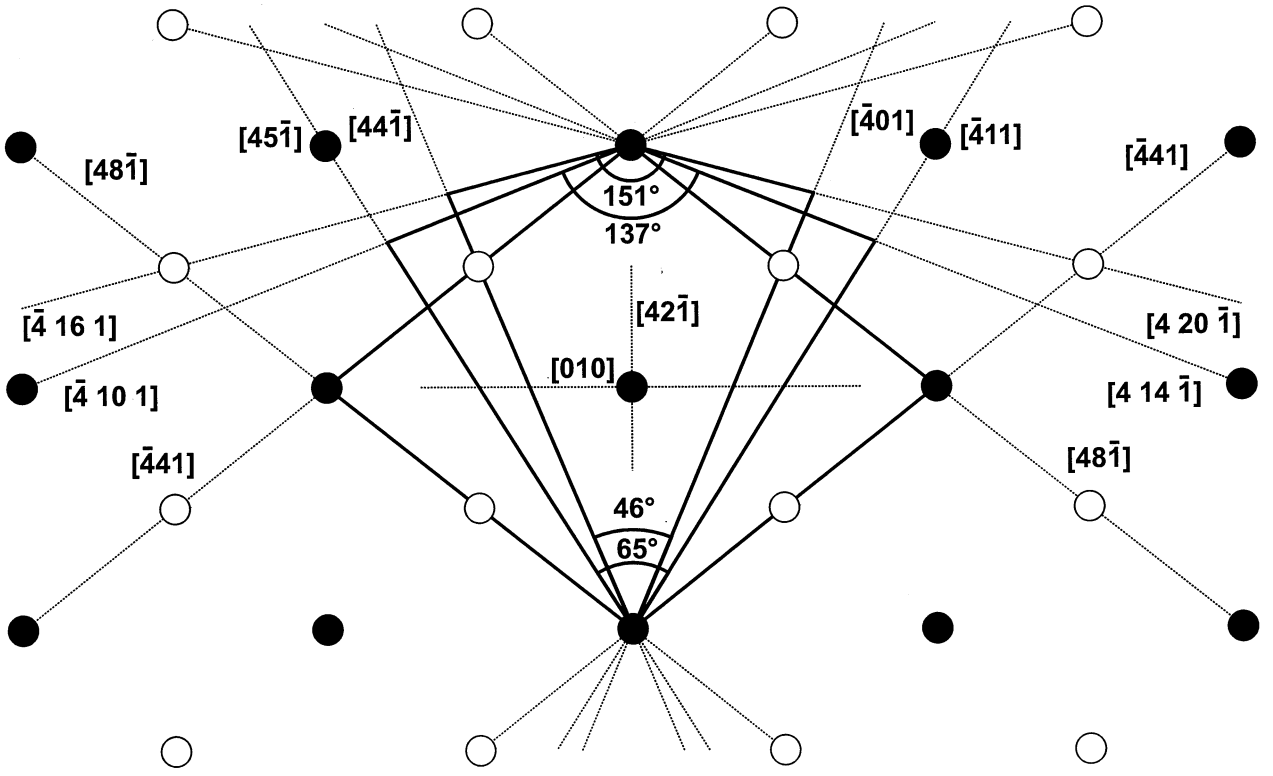

Fig. 9. Sketch showing low index directions on the (104) surface of calcite isotypes (cations and carbonate groups are represented by different circles). As can be seen from Figure 6, while decreasing pH to 2, the angle between obtuse steps starts to decrease from the rhombohedral directions [48$\bar{1}$] and [$\bar{4}$41] via [45$\bar{1}$] and [$\bar{4}$11] to ~49°. This angle corresponds roughly to the directions [44$\bar{1}$] and [$\bar{4}$01].

in the case of $g_{oo} \neq g_{oa}$ and $g \gg i_o$, an initial step vicinality of ~1° follows. This vicinality is clearly too small to be discerned by AFM images under the applied scanning conditions. Therefore, an increase of i_o relative to g_{oo} and g_{oa} (e.g., by a decrease of pH) can exert an additional influence on the increase of step vicinality.

3.2.3. Kink–Kink Separation

Although the kink dynamic model gives a semiquantitative description of the changes in step morphology caused by changes in solution pH, there are clearly limitations to the model. As we have shown above, the motion of rough steps can only be related indirectly to the detachment rate of kinks on straight steps. If surface or edge diffusion does not explain the failure of the kink dynamic model, then detachment rates are likely be governed by interactions between nearest, second-nearest, and possibly more distant neighbors. For example, at pH = 2, the angle between obtuse steps is 49 ± 5°. The steps, therefore, are oriented close to [44$\bar{1}$] and [$\bar{4}$01] (Fig. 9), and the distances between neighboring kinks along these steps reach values of two cation–anion distances (=0.59 nm; treating the carbonate group as a single anion unit). In this range of distances, coordination chemistry may become increasingly important, having an influence on the behavior of closely spaced kinks. On calcite, Shiraki et al. (2000) suggested detachment at kinks in pairs, i.e., carbonate group and metal ion detach together and dissociate in the aqueous phase. This detachment unit has a periodicity of two cation–anion distances, which supports the idea of coordinative influences. Detachment in pairs makes it possible that either the anion or the cation, exclusively, is exposed at the kink site by considering that the orientation of the pair might be relevant or that one ion may detach much slower than the other.

However, as shown in Figure 10 (left side of the pit), a g_{oa}-g_{oa} spacing of two cation–anion distances causes an alternating pattern in the type of ion directly exposed at the kinks. To circumvent this alternating pattern, steps oriented along [44$\bar{1}$] and [$\bar{4}$01] have, on average, alternating g_{oa}-g_{oa} distances of one and three intermolecular distances (Fig. 10, right side, solid line). However, segments with g_{oa}-g_{oa} distances of one cation–anion distance (=0.29 nm) are oriented along [42$\bar{1}$] and therefore can be either considered as segments of rough steps or as segments consisting of [42$\bar{1}$] PBC directions (Fig. 10, right side, broken line). Kink bunches that form rough steps might be stabilized to a certain degree by the development of stronger bonds, parallel to the step edge, reflected by the PBC theory. A detailed analysis and application of the PBC theory on the calcite (104) surface is given by Heijnen (1985) and Paquette and Reeder (1995). According to these analyses, the most probable step orientations on the (104) surface of calcite are along [48$\bar{1}$], [$\bar{4}$41], [42$\bar{1}$], and [010] (Fig. 9).

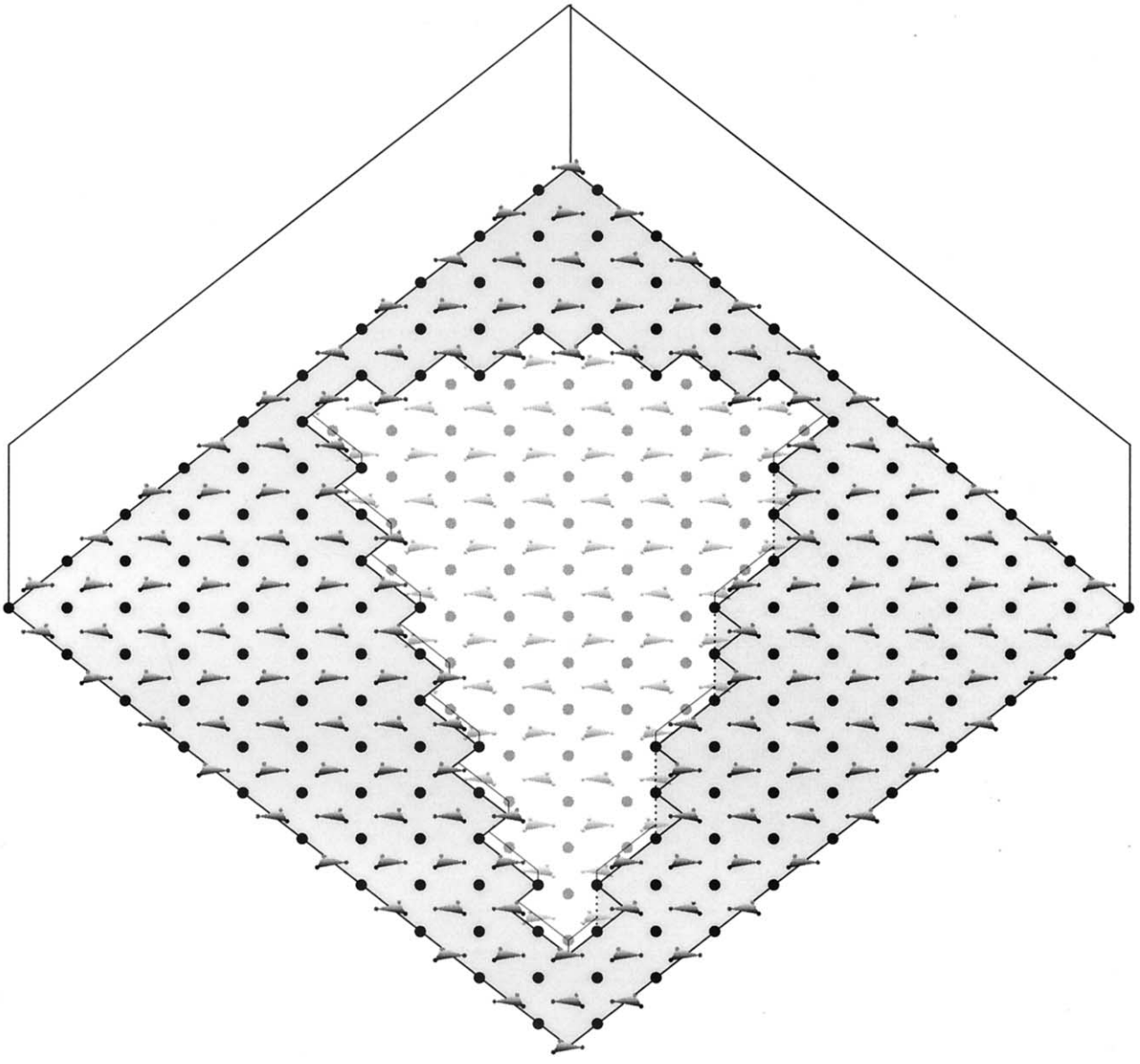

Fig. 10. Structure of straight steps within an etch pit at about pH = 2 on the magnesite (104) surface according to the kink dynamic model. On the left side, the obtuse step is composed of a regular array of kinks with kink–kink separations of two intermolecular distances. This array causes kinks to alternately consist of cations and anions. Any disturbance of this regular array, while maintaining the same step orientation, causes kink–kink separations of one intermolecular distance (≈0.3 nm) to occur, as shown on the right side of the pit.

4. CONCLUSION

At neutral to slightly acidic conditions, straight steps are oriented parallel to [48$\bar{1}$] and [$\bar{4}$41]. The equation $G = b[i(g_1 + g_2)]^{1/2}$ (Liang et al., 1996b) should therefore be applicable to the measured step velocities and kink detachment rates. The latter were estimated by measuring the step retreat of rough steps in HAFM image sequences and by assuming rough steps to consist of kink sites comparable to the corresponding kink sites at straight steps. However, KMC simulations show that the derived kink formation rate i is too large and the kink detachment rates g are too slow to obey the condition $g_1 \approx g_2 \gg i$, thus indicating an influence of kink density on detachment rate. Kink-density-dependent detachment rates can be explained by the tendency for step stabilization along the PBC directions [42$\bar{1}$] and [010], or by gradients in the surface concentration of adsorbed species (i.e., the analog to interstep interactions by concentration gradients; see, e.g., Chernov and Nishinaga, 1987).

Lowering the solution pH causes the straight steps to change orientation. This change can be described by a kink dynamic model based on an increased anisotropy of kink detachment rates at steps and/or a rough equalization of the slower kink detachment rate and the rate of double-kink formation. As a result, the slower detaching kinks accumulate along a step.

However, these decreased kink–kink separations along a step point toward coordinative influences that may stabilize steps along the PBC directions [42$\bar{1}$] and [010], which are also the directions rough steps approximately follow. Therefore, at low pH, all steps approach maximum kink density and—provided the exchange flux between the surface and the bulk fluid is large—dissolve at a maximum velocity limited by surface diffusion away from the step and/or by the kink detachment rate, which is then a function of the step coordination environment. In the next step, therefore, unraveling the specific role of magnesium in its coordination environment vs. the role of calcium on the isotype calcite surfaces might clarify mechanistic aspects of the "magnesite problem."

Acknowledgments—We thank Rolf Hollerbach (Mineralogisches Museum der Universität zu Köln) for providing samples. We thank the Deutsche Forschungsgemeinschaft (Jo 301/1-1,2 to G.J.) and the U.S. Department of Energy (KC040302 to K.G.K., and DE-FG03-96SF14623/A000 and DE-FG07-99ER15019 to C.M.E.) for financial support.

Associate editor: P. A. Maurice

REFERENCES

Britt D. W. and Hlady V. (1997) In-situ atomic force microscope imaging of calcite etch pit morphology changes in undersaturated and 1-hydroxyethylidene-1,1diphosphonic acid poisoned solutions. *Langmuir* **13,** 1873–1876.

Burton W. K., Cabrera N., and Frank F. C. (1951) The growth of crystals and the equilibrium structure of their surfaces. *Phil. Trans. R. Soc. Lond. A* **243**, 299–358.

Chernov A. A. and Nishinaga T. (1987) Growth shapes and their stability at anisotropic interface kinetics: Theoretical aspects for solution growth. In *Morphology of Crystals, Part A* (ed. I. Sunagawa), pp. 207–267. Terra.

Chou L., Garrels R. M., and Wollast R. (1989) Comparative study of the kinetics and mechanisms of dissolution of carbonate minerals. *Chem. Geol.* **78,** 269–282.

Compton R. G., Pritchard K. L., Unwin P. R., Grigg G., Silvester P., Lees M., and House W. A. (1989) The effect of carboxylic acids on the dissolution of calcite in aqueous solution. *J. Chem. Soc. Faraday Trans. 1* **85,** 4335–4366.

de Leeuw N. H., Parker S. C., and Harding J. H. (1999) Molecular dynamics simulation of crystal dissolution from calcite steps. *Phys. Rev. B* **60,** 13792–13799.

Fenter P., Geissbühler P., DiMasi E., Srajer G., Sorensen L. B., and Sturchio N. C. (2000) Surface speciation of calcite observed in situ by high-resolution X-ray reflectivity. *Geochim. Cosmochim. Acta* **64,** 1221–1228.

Frank F. C. (1974) Nucleation controlled growth on a one-dimensional growth of finite length. *J. Cryst. Growth* **22,** 233–236.

Gratz A. J., Hillner P. E., and Hansma P. K. (1993) Step dynamics and spiral growth on calcite. *Geochim. Cosmochim. Acta* **57,** 491–495.

Hartman P. and Perdok W. G. (1955) On the relations between structure and morphology of crystals. *Acta Cryst.* **8,** 49–52.

Heijnen W. M. M. (1985) The morphology of gel grown calcite. *N. Jb. Mineral. Mh.* **1985,** 357–381.

Higgins S. R., Eggleston C. M., Knauss K. G., and Boro C. O. (1998) A hydrothermal atomic force microscope for imaging in aqueous solution up to 150°C. *Rev. Sci. Instrum.* **69,** 2994–2998.

Hillner P. E., Gratz A. J., Manne S., and Hansma P. K. (1992) Atomic-scale imaging of calcite growth and dissolution in real time. *Geology* **20,** 359–362.

Jordan G. and Rammensee W. (1998) Dissolution rates of calcite (10$\bar{1}$4) obtained by scanning force microscopy: Microtopography-based dissolution kinetics on surfaces with anisotropic step velocities. *Geochim. Cosmochim. Acta* **62,** 941–947.

Keith R. E. and Gilman J. J. (1960) Dislocation etch pits and plastic deformation in calcite. *Acta Metal.* **8,** 1–10.

Lauritzen J. I. (1973) Effect of a finite substrate length upon polymer crystal lamellar growth rate. *J. Appl. Phys.* **44,** 4353–4359.

Liang Y. and Baer D. R. (1997) Anisotropic dissolution at the $CaCO_3$ (10$\bar{1}$4)-water interface. *Surf. Sci.* **373,** 275–287.

Liang Y., Lea A. S., Baer D. R., and Engelhard M. H. (1996a) Structure of the cleaved $CaCO_3$ (10$\bar{1}$4) surface in an aqueous environment. *Surf. Sci.* **351,** 172–182.

Liang Y., Baer D. R., McCoy J. M., and LaFemina J. P. (1996b) Interplay between step velocity and morphology during the dissolution of $CaCO_3$ surface. *J. Vac. Sci. Technol. A* **14,** 1368–1375.

Liang Y., Baer D. R., McCoy J. M., Amonette J. E., and LaFemina J. P. (1996c) Dissolution kinetics at the calcite–water interface. *Geochim. Cosmochim. Acta* **60,** 4883–4887.

Lippmann F. (1973) *Sedimentary Carbonate Minerals.* Springer.

McCoy J. M. and LaFemina J. P. (1997) Kinetic Monte Carlo investigation of pit formation at the $CaCO_3$ (1014) surface–water interface. *Surf. Sci.* **373,** 288–299.

Paquette J. and Reeder J. R. (1995) Relationship between surface structure, growth mechanism, and trace element incorporation in calcite. *Geochim. Cosmochim. Acta* **59,** 735–749.

Park N. S., Kim M. W., Langford S. C., and Dickinson J. T. (1996) Tribological enhancement of $CaCO_3$ dissolution during scanning force microscopy. *Langmuir* **12,** 4599–4604.

Pokrovsky O. S. and Schott J. (1999) Processes at the magnesium-bearing carbonate/solution interface. II. Kinetics and mechanism of the magnesite dissolution. *Geochim. Cosmochim. Acta* **63,** 881–897.

Pokrovsky O. S., Schott J., and Thomas F. (1999) Processes at the magnesium-bearing carbonate/solution interface. I. A surface speciation model for magnesite. *Geochim. Cosmochim. Acta* **63,** 863–880.

Shiraki R., Rock P. A., and Casey W. H. (2000) Dissolution kinetics of calcite in 0.1 M NaCl solution at room temperature: An atomic force microscopic (AFM) study. *Aquat. Geochem.* **6,** 87–108.

Stipp S. L. S., Eggleston C. M., and Nielsen B. S. (1994) Calcite surface structure observed at microtopographic and molecular scales with atomic force microscopy (AFM). *Geochim. Cosmochim. Acta* **58,** 3023–3033.

Teng H. H. and Dove P. M. (1997) Surface site–specific interactions of aspartate with calcite during dissolution: Implications for biomineralization. *Am. Mineral.* **82,** 878–887.

Thomas J. M. and Renshaw G. D. (1965) Dislocations in calcite and some of their chemical consequences. *Trans. Faraday Soc.* **61,** 791–796.